Ionics (2013) 19:63–69
DOI 10.1007/s11581-012-0704-1

ORIGINAL PAPER

Hydrothermal synthesis of $LiMnO_2$ microcubes for lithium ion battery application

Huan Xu · Jing Sun · Lian Gao

Received: 14 February 2012 / Revised: 19 March 2012 / Accepted: 22 March 2012 / Published online: 13 April 2012

Abstract Two kinds of $LiMnO_2$ microcubes were successfully synthesized by hydrothermal method using solid or hollow Mn_2O_3 microcubes as precursors. One was made up of nanoparticles varying in size and the other was made up of interlaced polygonal nanoplates with the thickness of 70 nm. Both kinds of $LiMnO_2$ microcubes were characterized by X-ray diffraction, scanning electron microscopy, and transmission electron microscopy. Charge–discharge curves were carried out to investigate their electrochemical properties. $LiMnO_2$ microcubes with interlaced nanoplates showed much better capacities than the ones with nanoparticles indicating it is more suitable for application in the lithium ion batteries. The former material could deliver the capacities of 197 and 134 mAh/g at 0.1 and 1 C, respectively. And its capacity fading after 50 cycles did not exceed 7 %. The excellent electrochemical performance of the former material could be ascribed to the smaller size which could shorten the path length for lithium ion transport and increase the electrode and electrolyte contact.

Keywords Cathodes · Electrochemical characterization · Li-ion battery · Electrodes

Introduction

The secondary lithium ion batteries have been widely utilized as the portable power source in electronics revolution [1–7]. $LiCoO_2$ introduced by Sony Corporate in 1991 was the first successfully commercial cathode material for the lithium ion batteries. However, its high cost and toxicity have pushed extensive research pursuing alternative cathodes. The Li–Mn–O-based systems including layered $LiMnO_2$ and spinel $LiMn_2O_4$ have attracted attention as cathode materials because of low cost and environmental advantages. $LiMn_2O_4$ has been studied a lot as a cathode material and shown good cycle performance [8–10]. Another cathode, $LiMnO_2$, with similar layered structure to $LiCoO_2$, has a higher theoretical discharge capacity of 285 mAh/g, almost twice as that of spinel $LiMn_2O_4$. Therefore, it is generally believed that $LiMnO_2$ would be a superior cathode material for the lithium ion batteries.

Up to the present, there are a lot of methods employed to prepare $LiMnO_2$ such as solid-state reaction [11], microwave-assisted process [12], micro-emulsion preparation [13], hydrothermal treatment [12, 14–17], and so on. Among the various attempts tried in the past few years, hydrothermal synthesis is an effective method for preparing $LiMnO_2$ cathode, especially on the morphology control. Zhou et al. [15] and Xiao et al. [16] successfully prepared $LiMnO_2$ nanorods keeping the morphology of MnOOH precursors by hydrothermal process. At the same time, lots of researches demonstrated that the smaller particle size of $LiMnO_2$ could shorten the path length for lithium ion transport and increase the electrode and electrolyte contact which were benefits for improving the rate performance and cycling stability [12, 15–17].

Here, we used hydrothermal method and took solid or hollow Mn_2O_3 microcubes constituted by nanoparticles as precursors to control the macroscopical morphology of $LiMnO_2$ and seek for the new microstructure favoring electrochemical performance. The scheme of the synthesis route was shown in Fig. 1. First, $MnCO_3$ microcubes were

H. Xu · J. Sun (✉) · L. Gao
The State Key Laboratory of High Performance Ceramics and Superfine Microstructures, Graduate School, Shanghai Institute of Ceramics, Chinese Academy of Sciences,
1295 Dingxi Road,
Shanghai 200050, People's Republic of China
e-mail: jingsun@mail.sic.ac.cn

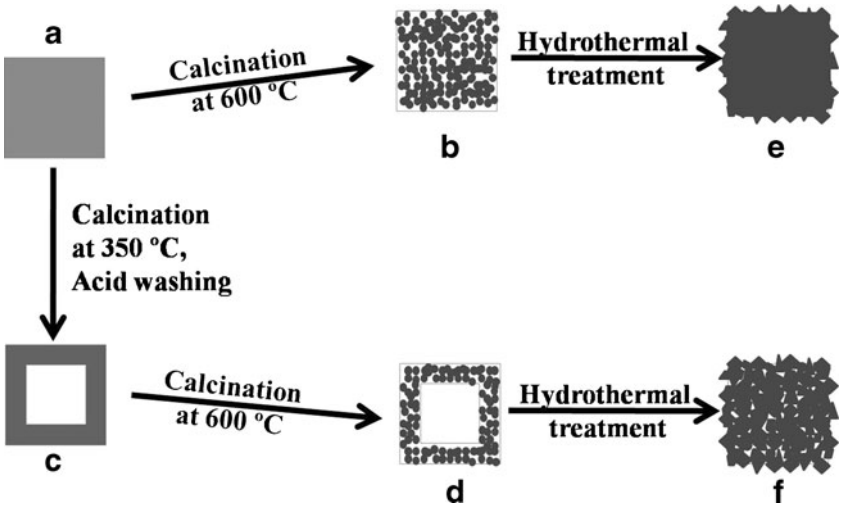

Fig. 1 Schematic illustration of the preparation of the final $LiMnO_2$ microparticles starting with the $MnCO_3$ microcubes (**a**). Solid Mn_2O_3 microcubes (**b**) were prepared after calcinating directly at 600 °C, while hollow Mn_2O_3 microcubs (**d**) were gained after calcinating hollow MnO_2 microcubes (**c**). $LiMnO_2$ microcubes (**e**) made up of nanoparticles were formed after hydrothermal treatment taking **b** as the precursors, while $LiMnO_2$ microcubes (**f**) made up of interlaced polygonal nanoplates were gained taking **d** as the precursor

prepared as shown in Fig. 1a. After calcinating $MnCO_3$ microcubes directly at 600 °C, the Mn_2O_3 microcubes were prepared (Fig. 1b), while the hollow Mn_2O_3 microcubes (Fig. 1d) were gained with hollow MnO_2 microcubes (Fig. 1c) as the intermediate. $LiMnO_2$ microcubes (Fig. 1e) made up of nanoparticles was formed after hydrothermal treatment taking solid Mn_2O_3 microcubes as the precursors, while $LiMnO_2$ microcubes (Fig. 1f) made up of interlaced polygonal nanoplates was gained taking hollow Mn_2O_3 microboxes as the precursors. The electrochemical tests indicated that $LiMnO_2$ microcubes with interlaced polygonal nanoplates showed much higher capacities at various current densities than $LiMnO_2$ microcubes with nanoparticles. Even more the capacity of $LiMnO_2$ microcubes with interlaced polygonal nanoplates at 1 C reached 134 mAh/g, much better than the reported results.

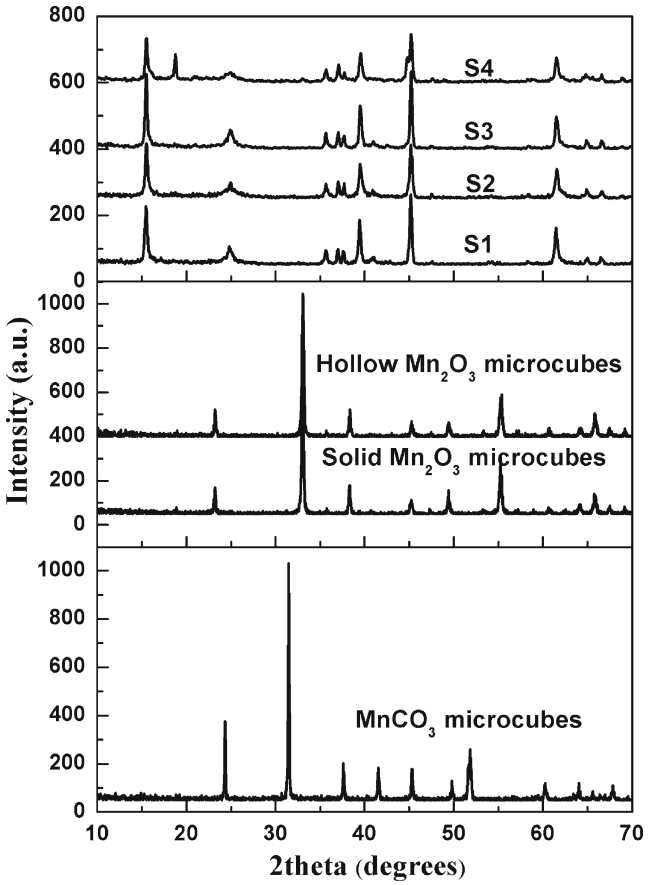

Fig. 2 XRD patterns of $MnCO_3$, solid and hollow Mn_2O_3 microcubes, S1, S2, S3, and S4

Experimental

All chemicals were of analytical grade and used as received.

The synthesis of $MnCO_3$ microcubes were based on the previous work of Lu's group [18]. In brief, $KMnO_4$ (0.948 g) was dissolved in distilled water (30 mL) and then added to an aqueous solution (30 mL) containing sucrose (0.75 g). The mixture was stirred for 20 min and then transferred to an autoclave (80 mL in volume) and hydrothermally treated at 150 °C for 24 h. The resultant precipitate was washed with distilled water and then was dried at 60 °C overnight to obtain the as-prepared $MnCO_3$ sample.

Of the as-prepared $MnCO_3$, 2.5 g was calcined in a furnace at 350 °C for 2 h with a heating rate of 5 °C/min in air. The product was washed in 0.1 M H_2SO_4 (450 mL) under stirring for 4 h. The resultant sample was filtered, washed with distilled water, and dried at 60 °C overnight to obtain the hollow MnO_2 microcubes. 1 g of as-prepared $MnCO_3$ sample and hollow MnO_2 microcubes were calcined at 600 °C with a heating rate of 5 °C/min for 24 h in air to obtain the solid and hollow Mn_2O_3 microcubes, respectively.

Of the as-prepared solid or hollow Mn_2O_3, 0.5 g microcubes was added to an autoclave containing 2 M LiOH solvent (60 mL) and 0.01 g glucose and hydrothermally treated at 160 °C for 12 h. The glucose was added to prevent

the formation of the Li_2MnO_3 impure phase. The products were washed with distilled water, dried at 60 °C overnight and labeled as S1 and S2, respectively. $LiMnO_2$ products S3 or S4 were prepared taking solid or hollow Mn_2O_3 microcubes as precursors but without adding glucose during the hydrothermal process.

Powder X-ray diffraction (XRD) patterns were recorded on a Rigaku D/MAX-2250 V diffractometer using Cu Ka radiation (λ=1.5418 Å, 40 kV, and 40 mA). Field-emission scanning electron microscope (FE-SEM) was performed on Hitachi S-4800 for sample S2 and on JSM-6700F for S1. Transmission electron microscopy (TEM) images were performed on a JEOL (JEM-2100F) microscope with an accelerating voltage at 200 kV. Nitrogen adsorption–desorption isotherms at 77 K were carried out on ASAP 2010.

The electrochemical properties of the $LiMnO_2$ samples as the positive electrode used in Li-ion batteries were evaluated using coin type cells with lithium metal as the counter electrode and Celgard 2500 as the separator. The working electrode was fabricated by mixing the active material, acetylene black, and polyvinylidene fluoride with a weight ratio of 80:10:10. The loading of the active material was ~1.06 mg/cm^2. The electrolyte (Beijing Institute of chemical reagents) was 1 M $LiPF_6$ in ethylene carbonate and diethyl carbonate (EC/DEC, 1:1, *v*/*v*). Cell assembly was carried out in a glove box filled with highly pure argon gas. The electrode activities were measured using a CT2001 battery tester. The galvanostatic charge/discharge experiments were performed between 2.0 and 4.5 V at different current densities.

Results and discussion

The successful synthesis of $MnCO_3$ sample is testified by the XRD pattern given in Fig. 2 and all of the diffraction peaks correspond to the pure rhombohedral phase of $MnCO_3$ (JCPDS no. 44-1472). The post-treatment of the as-prepared $MnCO_3$ resulted in the formation of Mn_2O_3 phase (Fig. 2; JCPDS no. 41-1442). When the glucose was not added during the hydrothermal process for $LiMnO_2$, samples S3 and S4 were prepared taking solid and hollow Mn_2O_3 microcubes as precursors respectively and their XRD patterns were shown in Fig. 2. It can be seen that S3 showed pure $LiMnO_2$ phase (JCPDS no. 35-0749), but a sharp peak at 18.6° attributed to the Li_2MnO_3 impure phase appeared for S4, indicating that Mn^{3+} was more easily oxidized to Mn^{4+} during the hydrothermal process for hollow Mn_2O_3 microcubes than solid Mn_2O_3 microcubes, implying that hollow Mn_2O_3 microcubes were more chemical active than solid Mn_2O_3 microcubes. The XRD patterns of S1 and S2 prepared with glucose added shown in Fig. 2 as well correspond to the final $LiMnO_2$ products (JCPDS no. 35-0749). No impure phase was detected, indicating that adding glucose can effectively prevent the formation of the Li_2MnO_3 impure phase. Figure 3 presents typical SEM and TEM images of the as-prepared precursors. The as-prepared $MnCO_3$ sample had solid micrometer-sized cube-like shape, as shown in Fig. 3a. After calcinating $MnCO_3$ at 600 °C, porous microcubes formed (Fig. 3b). Figure 3c shows the TEM image of hollow MnO_2 microcubes obtained by acid

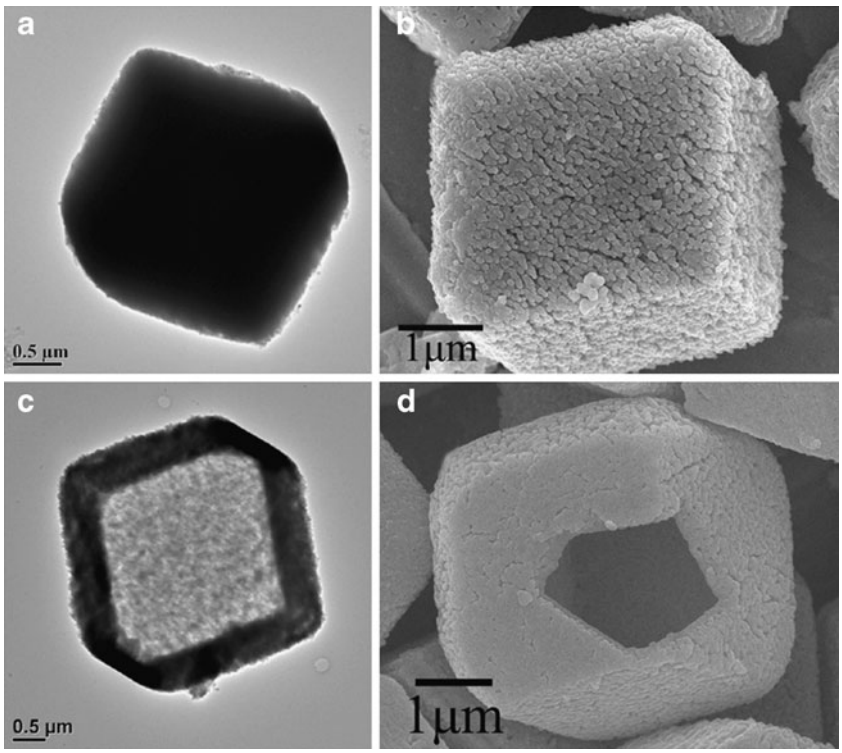

Fig. 3 TEM images of the as-prepared $MnCO_3$ microcubes (**a**) and hollow MnO_2 microcubes (**c**); SEM images of solid (**b**) and hollow (**d**) Mn_2O_3 microcubes

washing the $MnCO_3$ microcubes after calcination at 350 °C for 2 h. The further calcination of the hollow MnO_2 microcubes at 600 °C resulted in the formation of hollow Mn_2O_3 microcubes (Fig. 3d).

Figure 4 presents typical SEM and TEM images of the final $LiMnO_2$ products S1and S2. They still preserved general microcubic shape, but the edges and corners became vague. It can be seen that S1 was made up of hundreds of nanoparticles varying in size (Fig. 4a) and some of the nanoparticles had the plate-like morphologies. But in general, the shapes of the nanoparticles were anomalous. However, it can be seen that S2 consisted of interlaced polygonal nanoplates as shown in the inset of Fig. 4c. The thickness of the interlaced polygonal nanoplates was about 70 nm (Fig. 4c) and the interspaces between the interlaced polygonal nanoplates could store electrolyte which would have positive effect on the electrochemical performances. The different morphologies of S1and S2 could be attributed to the different Mn_2O_3 precursors. The more chemical active hollow Mn_2O_3 microcubes were apt to transform to $LiMnO_2$ microcubes constituted by the interlaced polygonal nanoplates during the hydrothermal process with LiOH and glucose. The TEM images (Fig. 4b and d) of S1 and S2 proved the microcubes with vague edges and no hollow structure had been observed for these two samples. A high-resolution TEM image (Fig. 4e) of S2 indicates that the microcubes are highly crystalline. Obvious grain boundaries can be seen as well and we choose a region marked by

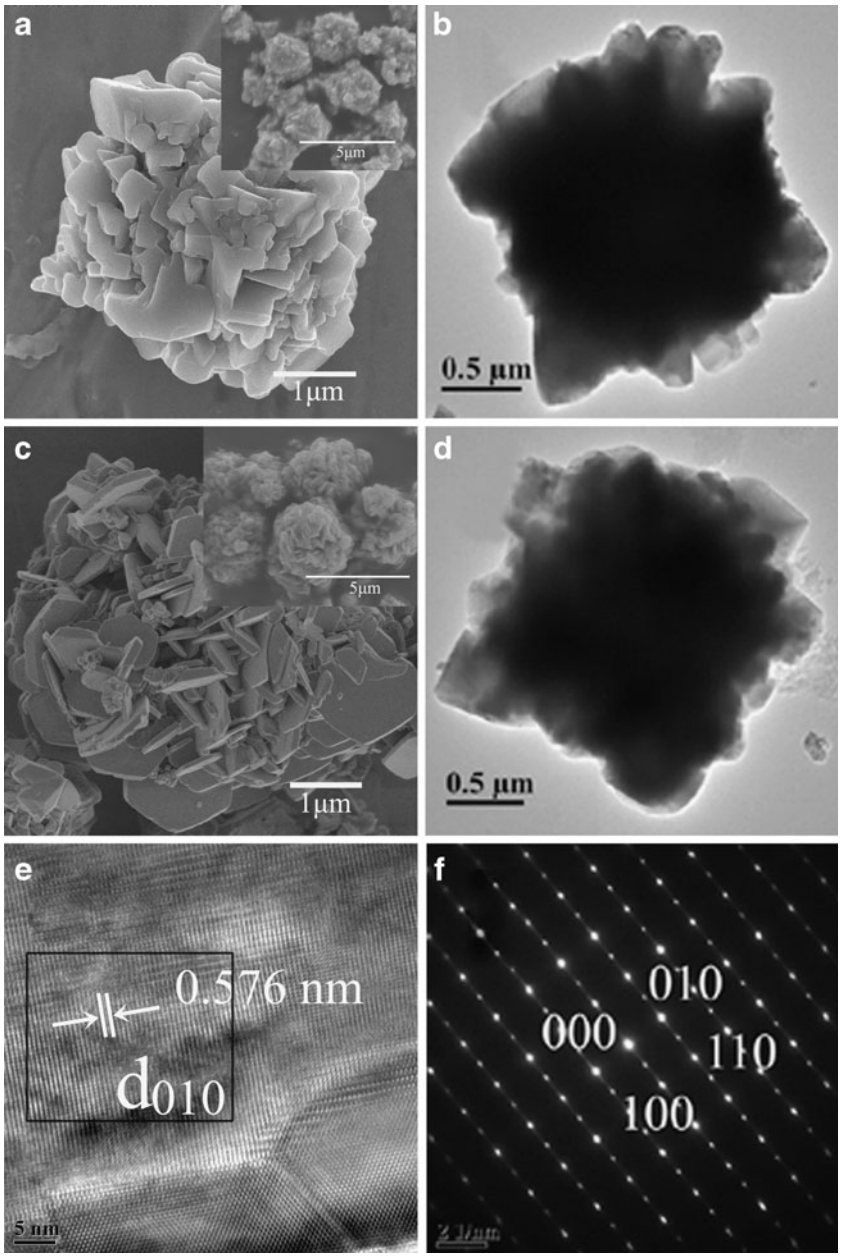

Fig. 4 Electron microscopy images of the final $LiMnO_2$ particles: **a** and **b** S1, **c**–**f** S2. The images of **a**, **c** are obtained from SEM while the others are obtained from TEM; inset of **a** and **c** shows the SEM images of S1 and S2, respectively, at low magnification

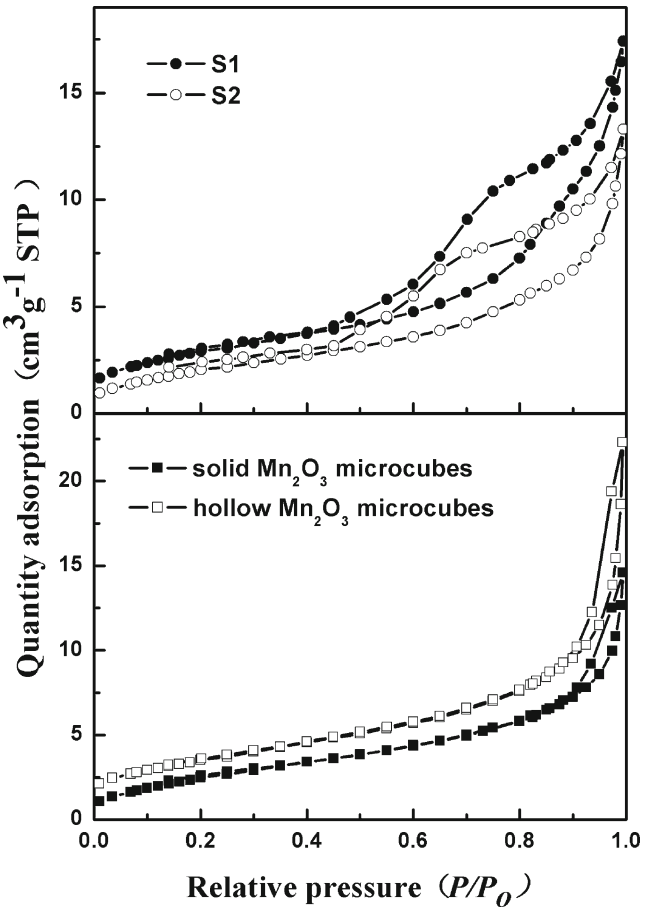

Fig. 5 Nitrogen sorption isotherms of solid and hollow Mn_2O_3 microcubes, S1 and S2

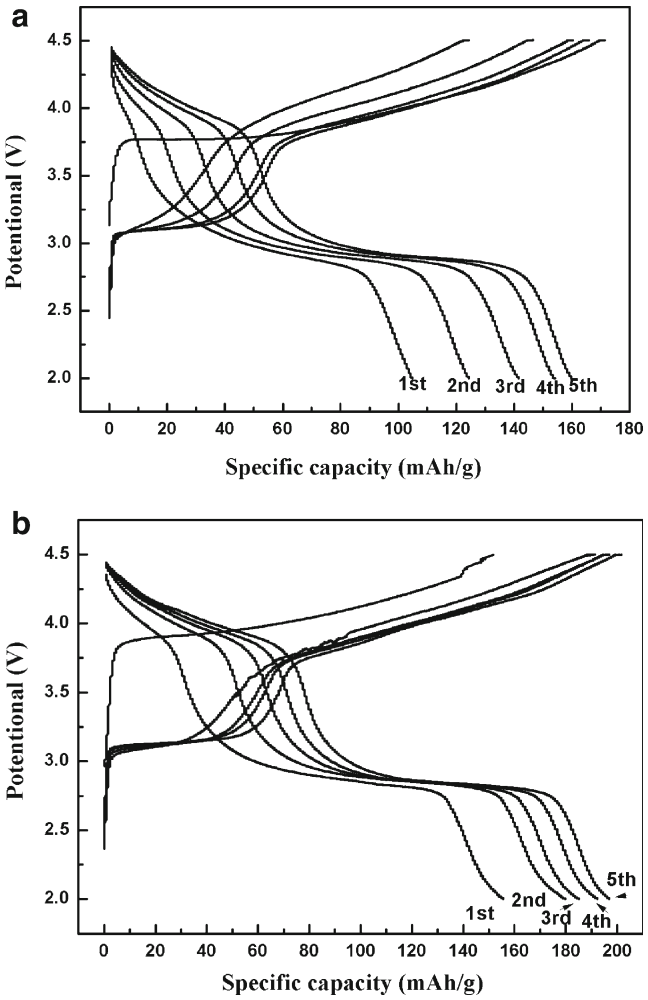

Fig. 6 The first five charge and discharge curves of **a** S1, **b** S2

black rectangle in Fig. 4e to further clarify the microstructure. The measured fringe spacing value in this region is 0.576 nm, corresponding to a d_{010} spacing. Typically, selected area electron diffraction pattern of the marked region is shown in Fig. 3f. The diffraction spots could be indexed as the layered $LiMnO_2$ with an orthorhombic structure. Nitrogen sorption measurements were performed at 77 K. The nitrogen sorption isotherms of Mn_2O_3 precursors and final $LiMnO_2$ products are shown in Fig. 5 and the corresponding pore textures are listed in Table 1. All the isotherms evidenced an IUPAC type IV behavior. The adsorption amount of N_2 for Mn_2O_3 precursors increased a lot above the relative pressure of 0.8, reflecting that the percentage of mesopores and micropores in the materials

Table 1 Pore texture properties of Mn_2O_3 precursors and $LiMnO_2$ products

Samples	S_{BET} (m^2/g)	V_t (cm^3/g)	D_{BJH} (nm)
Solid Mn_2O_3 microcubes	9.9	0.015	9.0
Hollow Mn_2O_3 microcubes	12.8	0.021	10.8
S1	10.8	0.022	8.0
S2	8.0	0.015	7.3

S_{BET} specific surface area, V_t total pore volume, D_{BJH} pore diameter calculated by BJH method

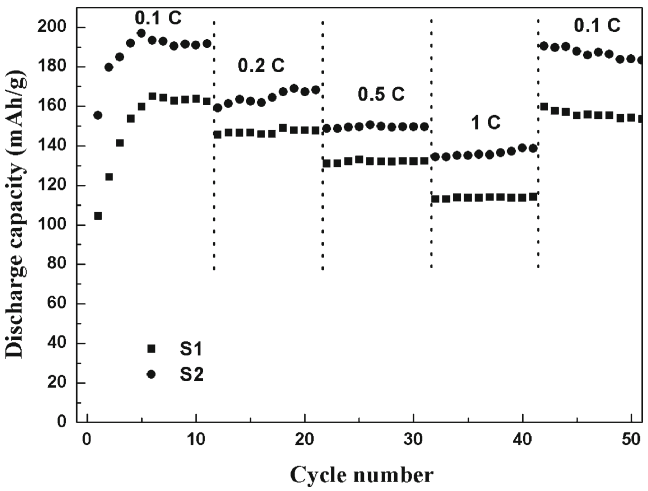

Fig. 7 Cycle performance of the final $LiMnO_2$ microcubes at different current densities in the potential range 2 and 4.5 V (vs. Li^+/Li)

was large. Hollow Mn_2O_3 microcubes had more specific surface area and total pore volume and bigger average pore diameter calculated by BJH method than solid Mn_2O_3 microcubes, which could be attributed to the hollow structure introduced by acid washing process. The hysteresis loop for $LiMnO_2$ products appeared at a broad relative pressure range (0.4–1.0), indicating that the pores in the materials were hierarchical. When solid Mn_2O_3 microcubes transformed to S1, the specific surface area increased from 9.9 to 10.8 m^2/g and the total pore volume increased from 0.015 to 0.022 cm^3/g. While when hollow Mn_2O_3 microcubes transformed to S2, the specific surface area decreased from 12.8 to 8.0 m^2/g and the total pore volume increased from 0.021 to 0.015 cm^3/g. The reason for the decline might be the disappearance of the hollow structure.

Figure 6 depicts the first five charge and discharge curves of S1 and S2 at a current load of 0.1 C. The initial charge/discharge capacities were 172/105 and 152/155 mAh/g for S1 and S2, respectively. The corresponding Coulombic efficiencies reached 61 and 102 %. Shu et al. [19] claimed that the irreversible capacity was due to the phase transition from $LiMnO_2$ to spinel $LiMn_2O_4$, which was confirmed by Kotschau and Dahn by in situ XRD measurement results [20, 21]. With increasing cycles for all the samples, the length of 4 V plateaus trends to increase implying continuous phase transition from $LiMnO_2$ to spinel $LiMn_2O_4$ [12, 16] and the discharge capacities of the four samples increased distinctly.

The discharge capacities reached maximum value of 165 and 197 mAh/g by the sixth and fifth cycle for S1 and S2, respectively (Fig. 7). Compared with other $LiMnO_2$ materials such as those reported by Xiao et al. [16] requiring four cycles, those by Zhou et al. [15] and by Wei et al. [22] requiring 12 and even 30 cycles, our materials were easy to be activated and quickly reached their maximum capacities. The discharge capacities as a function of discharge densities were evaluated and shown in Fig. 7, where the charge/discharge cycle was carried out 10 times at every current density. The capacities of S1 reached 147, 132, and 114 mAh/g, while the capacities of S2 attained 164, 150, and 134 mAh/g when the current density increased to 0.2, 0.5, and 1 C, respectively. So it is easy to distinguish that S2 shows much better capacities than S1 at various current densities. The $LiMnO_2$ microcubes showed the capacity of 160 for S1 and 190 mAh/g for S2, respectively, when the current density returns to 0.1 C. The capacity fading after 50 cycles, calculated by the discharge capacity of the 50th cycle divided by the maximum discharge capacity of the $LiMnO_2$ microcubes, did not exceed 7 %. It is worth to tell that the discharge capacities of S2 reached above 134 mAh/g at 1 C, much better than the capacity of about 90 mAh/g at 1 C reported by Ammundsen et al. [23] and 88 at 200 mA/g reported by Xiao et al. [16].

The outstanding performance of S2 indicates that it is more suitable for application in lithium ion batteries. The possible reason for this phenomenon could be the smaller particle size for S2. Its interlaced polygonal nanoplate morphology with the thickness of 70 nm has shortened the diffusion length for lithium ion compared with the morphology of nanoparticles varying in size for S1. Since the insertion of lithium ions to the $LiMnO_2$ materials is diffusion determinated, the short diffusion length favors the electrode kinetics and the charge–transport process in the charge/discharge cycles, thus the electrochemical properties of S2 were greatly improved [15].

Conclusions

$MnCO_3$ microcubes were prepared first and successfully transformed to solid or hollow Mn_2O_3 microcubes. Layered $LiMnO_2$ microcubes were synthesized by hydrothermal method. S1 prepared taking solid Mn_2O_3 microcubes as the precursor was made up of nanoparticles varying in size, while S2 prepared taking hollow Mn_2O_3 microcubes as the precursor was constituted by interlaced polygonal nanoplate with the thickness of 70 nm. S2 exhibited much better capacities than S1 at various current densities because of the smaller particle size which shortened the diffusion length and increased the electrode and electrolyte contact, indicating it is more suitable for application in the lithium ion batteries.

Acknowledgments This work is supported by National Basic Research Program of China (2012CB932303) and the National Natural Science Foundation of China (n. 50972153).

References

1. Tarascon JM, Armand M (2001) Issues and challenges facing rechargeable lithium batteries. Nature 414(6861):359–367
2. Okubo M, Hosono E, Kim J, Enomoto M, Kojima N, Kudo T, Zhou HS, Honma I (2007) Nanosize effect on high-rate li-ion intercalation in $LiCoO_2$ electrode. J Am Chem Soc 129 (23):7444–7452
3. Sun CW, Rajasekhara S, Goodenough JB, Zhou F (2011) Monodisperse porous $LiFePO_4$ microspheres for a high power li-ion battery cathode. J Am Chem Soc 133(7):2132–2135
4. Oh SH, Chung KY, Jeon SH, Kim CS, Cho WI, Cho BW (2009) Structural and electrochemical investigations on the $LiNi_{(0.5-x)}Mn_{(1.5-y)}M_{(x+y)}O_{(4)}$ (M=Cr, Al, Zr) compound for 5 V cathode material. J Alloy Compd 469(1–2):244–250
5. Liu GQ, Wen L, Liu GY, Tian YW (2010) Rate capability of spinel $LiCr_{(0.1)}Ni_{(0.4)}Mn_{(1.5)}O_{(4)}$. J Alloy Compd 501(2):233–235
6. Ying W, Sun B, Park J, Kim WS, Kim HS, Wang GX (2011) Morphology control and electrochemical properties of nanosize $LiFePO_4$ cathode material synthesized by co-precipitation combined with in situ polymerization. J Alloy Compd 509(3):1040–1044

7. Kim HJ, Kim JM, Kim WS, Koo HJ, Bae DS, Kim HS (2011) Synthesis of $LiFePO_4$/C cathode materials through an ultrasonic-assisted rheological phase method. J Alloy Compd 509(18):5662–5666
8. Lee HW, Muralidharan P, Ruffo R, Mari CM, Cui Y, Kim DK (2010) Ultrathin spinel $LiMn_2O_4$ nanowires as high power cathode materials for Li-ion batteries. Nano Lett 10(10):3852–3856
9. Ding YL, Xie JA, Cao GS, Zhu TJ, Yu HM, Zhao XB (2011) Single-crystalline $LiMn_2O_4$ nanotubes synthesized via template-engaged reaction as cathodes for high-power lithium ion batteries. Adv Funct Mater 21(2):348–355
10. Hirose S, Kodera T, Ogihara T (2010) Synthesis and electrochemical properties of Li-rich spinel type $LiMn_2O_4$ powders by spray pyrolysis using aqueous solution of manganese carbonate. J Alloy Compd 506(2):883–887
11. Li XL, Liu DJ, Zhang DW, Chen XY, Tian XL (2009) One-step synthesis and electrochemical behavior of $LiMnO_2$ and its composite from MnO_2 in the presence of glucose. J Phys Chem Solids 70(6):936–940
12. Ji HM, Yang G, Miao XW, Hong AQ (2010) Efficient microwave hydrothermal synthesis of nanocrystalline orthorhombic $LiMnO_2$ cathodes for lithium batteries. Electrochim Acta 55(9):3392–3397
13. Lu CH, Wang HC (2004) Reverse-microemulsion preparation and characterization of ultrafine orthorhombic $LiMnO_2$ powders for lithium-ion secondary batteries. J Eur Ceram Soc 24(5):717–723
14. Liu Q, Li YX, Hu ZL, Mao DL, Chang CK, Huang FQ (2008) One-step hydrothermal routine for pure-phased orthorhombic $LiMnO_2$ for Li ion battery application. Electrochim Acta 53 (24):7298–7302
15. Zhou F, Zhao XM, Liu YQ, Li L, Yuan CG (2008) Size-controlled hydrothermal synthesis and electrochemical behavior of orthorhombic $LiMnO_2$ nanorods. J Phys Chem Solids 69(8):2061–2065
16. Xiao XL, Wang L, Wang DS, He XM, Peng Q, Li YD (2009) Hydrothermal synthesis of orthorhombic $LiMnO_2$ nano-particles and $LiMnO_2$ nanorods and comparison of their electrochemical performances. Nano Res 2(12):923–930
17. He Y, Li RH, Ding XK, Jiang LL, Wei MD (2010) Hydrothermal synthesis and electrochemical properties of orthorhombic $LiMnO_2$ nanoplates. J Alloy Compd 492(1–2):601–604
18. Wang LZ, Tang FQ, Ozawa K, Chen ZG, Mukherj A, Zhu YC, Zou J, Cheng HM, Lu GQ (2009) A general single-source route for the preparation of hollow nanoporous metal oxide structures. Angew Chem Int Ed 48(38):7048–7051
19. Shu ZX, Davidson IJ, McMillan RS, Murray JJ (1997) Electrochemistry of $LiMnO_2$ over an extended potential range. J Power Sources 68(2):618–622
20. Myung ST, Komaba S, Kumagai N (2001) Orthorhombic $LiMnO_2$ as a high capacity cathode for lithium-ion battery synthesized by hydrothermal route at 170 degrees C. Chem Lett 1:80–81
21. Kotschau IM, Dahn JR (1998) In situ X-ray study of $LiMnO_2$. J Electrochem Soc 145(8):2672–2677
22. Wei YJ, Ehrenberg H, Bramnik NN, Nikolowski K, Baehtz C, Fuess H (2007) In situ synchrotron diffraction study of high temperature prepared orthorhombic $LiMnO_2$. Solid State Ion 178 (3–4):253–257
23. Ammundsen B, Paulsen J (2001) Novel lithium-ion cathode materials based on layered manganese oxides. Adv Mater 13(12–13):943–956